The APP intracellular domain forms nuclear multiprotein complexes and regulates the transcription of its own precursor

Ruth C. von Rotz[1], Bernhard M. Kohli[1], Jérôme Bosset[1], Michelle Meier[1], Toshiharu Suzuki[2], Roger M. Nitsch[1] and Uwe Konietzko[1,*]

[1]Division of Psychiatry Research, University of Zurich, August Forel-Str. 1, 8008 Zurich, Switzerland
[2]Laboratory of Neuroscience, Graduate School of Pharmaceutical Sciences, Hokkaido University, Kita-ku, Kita 12, Nishi-6, Sapporo, 060-0812, Japan
*Author for correspondence (e-mail: uwe.konietzko@bli.unizh.ch)

Accepted 24 May 2004
Journal of Cell Science 117, 4435-4448 Published by The Company of Biologists 2004
doi:10.1242/jcs.01323

Summary

The physiological functions of the beta-amyloid precursor protein (APP) may include nuclear signaling. To characterize the role of the APP adaptor proteins Fe65, Jip1b, X11α (MINT1) and the chromatin-associated protein Tip60, we analyzed their interactions by confocal microscopy and co-immunoprecipitations. AICD corresponding to S3-cleaved APP bound to Fe65 that transported it to nuclei and docked it to Tip60. These proteins formed AICD-Fe65-Tip60 (AFT) complexes that were concentrated in spherical nuclear spots. γ-Secretase inhibitors prevented AFT-complex formation with AICD derived from full-length APP. The APP adaptor protein Jip1b also transported AICD to nuclei and docked it to Tip60, but AICD-Jip1b-Tip60 (AJT) complexes had different, speckle-like morphology. By contrast, X11α trapped AICD in the cytosol. Induced AICD expression identified the APP-effector genes *APP, BACE, Tip60, GSK3β* and *KAI1*, but not the Notch-effector gene *Hes1* as transcriptional targets. These data establish a role for APP in nuclear signaling, and they suggest that therapeutic strategies designed to modulate the cleavage of APP affect AICD-dependent signaling.

Key words: AICD, Alzheimer's disease, Tip60, Fe65, γ-Secretase, Transcriptional regulation

Introduction

The amyloid precursor protein (APP) is a single-pass transmembrane protein that is involved in the pathophysiology of Alzheimer's disease (AD) (Selkoe, 1999). Successive proteolytic processing, with ectodomain shedding followed by intramembraneous cleavage (De Strooper, 2003; Sisodia and St George-Hyslop, 2002; Walter et al., 2001), generates beta-amyloid (Aβ) peptides; these aggregate to form β-amyloid plaques in the brains of patients with AD. A large body of genetic and cell biological evidence strongly argues for pathogenic activities of Aβ, including a role in the formation of neurofibrillary tangles (Gotz et al., 2001; Lewis et al., 2001). Initial clinical evidence in support of a pathogenic role of Aβ in humans was recently provided by the observation that antibodies against Aβ generated in response to vaccination slowed the rate of cognitive decline in patients with AD (Hock et al., 2002; Hock et al., 2003). Together, these findings led to the development of a large variety of different pharmacological and immunological approaches aiming at lowering brain levels of Aβ. Along with Aβ generation, intramembraneous proteolysis of APP also liberates the APP intracellular C-terminus (AICD) from the membrane. AICD was described long after the initial identification of APP (Passer et al., 2000), probably because of its rapid degradation after release from the membrane into the cytoplasm (Cupers et al., 2001a; Kimberly et al., 2001), in part by insulin degrading enzyme (Edbauer et al., 2002; Farris et al., 2003).

The analogy of APP processing to Notch receptor signaling suggested a possible function for AICD in nuclear signaling (De Strooper et al., 1999; Schroeter et al., 1998). In a seminal experiment, Cao and Südhof (Cao and Südhof, 2001) have used APP- and AICD-fusions with the yeast Gal4 transcription factor DNA-binding domain and observed transactivation activity for AICD. This was dependent on the APP-adaptor protein Fe65 (Duilio et al., 1991; Minopoli et al., 2001) and the Fe65-binding nuclear histone acetylase Tip60 (Sterner and Berger, 2000). However, the possibility remains that, in transient transfection assays, the transcription from reporter constructs could also occur in the cytosol. Fe65 has been shown to stabilize the intracellular domains of γ-secretase cleaved APP, APLP1 and APLP2, which together with Fe65, localized to the nuclear compartment (Kimberly et al., 2001; Walsh et al., 2003). These experiments suggested a role in nuclear signaling for the AICD.

To characterize the molecular requirements for the nuclear localization of AICD, we used inducible expression of fluorescently tagged AICD and cotransfection of AICD-adaptor proteins, followed by analysis via confocal microscopy and co-immunoprecipitation.

Materials and Methods

Cell culture

HEK293 cells were grown in DMEM supplemented with 10% fetal

bovine serum (Gibco, Basel, Switzerland). Transfections were done with Lipofectamin 2000 (Invitrogen, Basel, Switzerland) either on plastic culture dishes or on glass slide chambers (Falcon, Mettmenstetten, Switzerland) coated with polyornithine (10 μg/ml, Sigma, Buchs, Switzerland) and laminin (5 μg/ml, Invitrogen, Basel, Switzerland). For all experiments involving confocal microscopy cells were fixed with 4% paraformaldehyde in PBS 16 to 20 hours after transfection. At this time expression levels of transfected Fe65 were threefold higher than endogenous levels and transfected Tip60 led to a fivefold increase over expression in naive HEK293 cells as determined by western blotting. In experiments involving stable lines with inducible expression of citrine-AICD, the expression was induced the day before transfection, resulting in expression for 40 to 44 hours. In long-term experiments we observed no evidence of toxicity or apoptosis, as determined by TUNEL staining (Kit 1 684 817, Roche, Rotkreuz, Switzerland), for up to 5 days of induced expression of citrine-AICD. To inhibit γ-secretase either 1 μM DAPT or 10 μM L685,458 (Calbiochem, Lucerne, Switzerland) were added after transfection. SH-SY5Y neuroblastoma cells were grown in DMEM/F12 supplemented with 20% fetal bovine serum. For differentiation, cells were sequentially treated for 5 days with 5 μM retinoic acid (Sigma, Buchs, Switzerland) and for 5 days with 20 ng/ml BDNF (Peprotech, London, UK), with serum reduced to 2%, after which they were transfected identically to HEK293 cells.

Expression constructs

To construct an inducible expression vector we excised the Bombyx mori ecdyson receptor-VP16 fusion transactivator and response elements from a retroviral backbone (Suhr et al., 1998) and cloned them into plasmids with inverted repeats recognized by the sleeping beauty transposase (Ivics et al., 1997). Expression of the Bombyx transactivator was driven by a glyceraldehyde-3-phosphate dehydrogenase promotor excised *Hin*dIII/*Xba*I from a plasmid provided by Maria Alexander (Harvard Medical School, Cambridge, MA) (Alexander et al., 1988). The ecdyson response element was followed by a polylinker for the insertion of citrine-AICD and APP-citrine fusion proteins. The improved YFP citrine (Griesbeck et al., 2001) was a gift from R. Y. Tsien (University of California at San Diego, CA). For the citrine-AICD fusion protein, the C-terminal lysine of citrine was followed by a GPGAL spacer fused to valine50 (Aβ sequence) of the S3-cleaved APP C-terminal domain. For full-length APP, citrine was fused to the C-terminus of APP_{695}, either via a short spacer (APP-PGPRASLPVAT-citrine), or via a dual tandem HA tag (APP-PGPRSGYPYDVPDYATGYPYDVPDYATGDP-citrine).

Mouse Jip1b and human X11α with an N-terminal HA tag in pcDNA3.1 have been described previously (Taru et al., 2002a; Taru and Suzuki, 2004). Human Fe65 with an N-terminal HA tag in pcDNA3.1 was a gift from Konrad Beyreuther (ZMBH, Heidelberg, Germany). We exchanged the HA tag for myc or FLAG tags in Fe65 and Jip1b for some experiments. A CFP-Tip60 (human Tip60) fusion protein in pEGFP-C2 (Clontech, Basel, Switzerland) was provided by Craig Robson (Northern Institute for Cancer Research, Newcastle, UK) (Gaughan et al., 2001) and the GFP was substituted by CFP via *Nhe*I and *Bsr*GI sites. Site-directed mutagenesis (Quick Change Mutagenesis Kit, Stratagene, Amsterdam, The Netherlands) was performed to mutate the NKSY of Tip60 to NASA. All cloned and mutagenised constructs were verified by sequencing (ABI Prism 310, Perkin Elmer, Hühnenberg, Switzerland).

Staining and antibodies

Primary antibodies were anti-HA tag, high affinity (Roche, Rotkreuz, Switzerland), anti-APP C-terminus (8717, Sigma, Buchs, Switzerland), 6E10 (Signet, Dedham, MA), 22C11 (MAB348, Chemicon, Lucerne, Switzerland), anti-Fe65 (sc-19751, Santa Cruz, Nunningen, Switzerland), anti-Jip1, 2 (34-5300, Zymed, Basel, Switzerland), anti-GAPDH (A6457, Molecular Probes, Lucerne, Switzerland), anti-Tip60 (Upstate, Lucerne, Switzerland), anti-myc tag (Upstate, Lucerne, Switzerland), anti-FLAG tag (Sigma, Buchs, Switzerland) and anti-GFP (Upstate, Lucerne, Switzerland). All washings were performed with TBS, 0.05% TritonX-100, for blocking and antibody incubation 5% normal horse and 5% normal goat serum were added. All secondary antibodies were highly purified for species cross-reactivity (Jackson Labs, Bar Harbor, Maine) labeled with Cy3 or Cy5 dyes. In control experiments, omitting the respective primary antibody showed no staining of antibodies from other species. For nuclear staining we used DRAQ5 (Biostatus, Leicestershire, UK), which is an anthraquinone that has a high affinity for DNA, can be excited by the 633 nm laser line, and emits in the far red spectrum.

Confocal microscopy and fluorescence resonance energy transfer (FRET) analysis

All images were acquired on a Leica TCS/SP2 confocal microscope (Leica, Wetzlar, Germany) with a 63× water immersion objective. The Argon Laser line of 458 nm was used to excite CFP (PMT window: 465-485 nm) and the 514 nm line to excite citrine. The PMT window for detecting citrine was 525-580 nm when co-stained with Cy5, and 525-545 nm when co-stained with Cy3 to prevent the detection of Cy3 in the citrine channel. A 543 nm HeNe laser was used to excite Cy3 (PMT window: 553-600 nm). A 633 nm HeNe laser was used to excite Cy5 (PMT window: 655-710 nm) or DRAQ5 (PMT window: 650-800 nm). Between 5 and 15 sections in the z-axis (xy-mode) or y-axis (xz-mode) were acquired, and maximum projections of the sections encompassing the nucleus were performed.

Raw FRET was measured by exciting CFP with the 458 nm laser line and measuring sensitized citrine emission at 525-555 nm in single sections. Values for CFP bleach-through (0.24) and citrine cross-excitation (0.07) were determined in cells expressing either fluorophore alone. No pixel shift was observed and background fluorescence was negligible. After sequentially measuring raw FRET, CFP and citrine fluorescence NFRET calculations were performed as described previously (Xia and Liu, 2001). For bleaching experiments the image was zoomed four- to sixfold and the citrine fluorescence in single nuclei was bleached with the 514 nm line at 100% laser intensity.

Western blotting and immunoprecipitation

Stably transfected HEK293 cells were induced to express citrine-AICD, and were cotransfected with Fe65 or Tip60 expression constructs. For the preparation of nuclear protein extracts, cells were collected in hypotonic buffer 24 hours after cotransfection [10 mM Hepes, 10 mM KCl, 5 mM $MgCl_2$, 1 mM DTT, 1 mM PMSF, 2.5× Roche Complete protease inhibitor mix without EDTA (Roche, Rotkreuz, Switzerland), 5 mM phenantroline (PNT) (Sigma, Buchs, Switzerland)], swollen on ice for 15 minutes and passed through a 22 G syringe. Sucrose was added to a final concentration of 0.25 M followed by centrifugation for 5 minutes at 500 ***g***.

Pellets were resuspended in wash buffer (25 mM sucrose pH 7.5, 6 mM $MgCl_2$, 10 mM TrisHCl (pH 7.4), 0.1% TritonX-100, 1 mM PMSF, 5 mM PNT, 2.5× Roche Complete without EDTA) and centrifuged again at 500 ***g*** (repeated twice). Nuclei were solubilized for 1 hour in wash buffer supplemented with 1% TritonX-100 and mechanically disrupted by passing through a 26 G syringe.

Nuclear protein extracts were incubated over night at 4°C with specific antibodies coupled to protein G sepharose (Amersham, Otelfingen, Switzerland) in the presence of 0.2% TritonX-100. Precipitated proteins were washed and boiled in LDS-containing loading buffer, separated by 4-12% Nupage Tris-PAGE (Invitrogen, Basel, Switzerland) with MOPS running buffer. Blotting onto PVDF membranes (Invitrogen, Basel, Switzerland) was followed by enhanced chemiluminescense detection (Amersham, Otelfingen, Switzerland) or SuperSignal West Femto (Pierce, Lausanne, Switzerland).

Whole cell extracts from HEK293 were isolated in a PBS lysis buffer containing 1% Triton X-100, supplemented with 1 mM PMSF and Roche Complete Protease inhibitor mix with EDTA (Roche, Rotkreuz, Switzerland). Extracts were separated on 10-20% Tricine gels (Invitrogen, Basel, Switzerland), blotted on nitrocellulose membranes (0.45 μm; Biorad, Reinach, Switzerland) or Protran BA 79 Cellulosenitrate membranes (0.1 μm; Schleicher & Schuell, Dassel, Germany) and detected by enhanced chemiluminescence as above.

Reverse transcription (RT) and quantitative real-time PCR

Total RNA was isolated from clonal HEK293 lines with TRIzol (Invitrogen, Basel, Switzerland). Cells were grown either with or without the induction of citrine-AICD expression for 48 hours. First-strand cDNA synthesis was performed using the SuperScript First-Strand Synthesis System for RT-PCR (Invitrogen, Basel, Switzerland) according to the manufacturer's protocol. Real-time-PCR was performed on the TaqMan using SYBR Green (Applied Biosystems, Rotkreuz, Switzerland). The amplification mixtures contained 0.8 ng/μl Template cDNA, 1× SYBR Green PCR buffer, 3 mM $MgCl_2$, 1.25 mM dNTPs, 0.25 U AmpErase, 0.75 U AmpliTaq Gold, 10 μM Forward Primer and 10 μM Reverse Primer. The Primers were designed to amplify the 3′ end to middle of the ORF part, except for the citrine-AICD fusion protein where they spanned the fusion border. Primer sequences are: GAPDH (sense: TGGGCTACACTGAGCACCAG; reverse: CAGCGTCAAAGGTGGAGGAG), PGK (sense: TGAAGGACTGTGTAGGCCCAG; reverse: TTCTTCCTCCACATGAAAGCG), KAI1 (sense: CTACAACAGCAGTCGCGAGG; reverse: CGCAGCACTTCACCTGAGC), GSK3β (sense: ACAAGGACGGCAGCAAGGT; reverse: ACTTCTTGTGGCCTGTCTGG), APP (sense: ACCAACTTGCATGACTACGGC; reverse: CACACAAACTCTACCCCTCGG) ADAM10 (sense: CTCCAC AGCCCATTCAGCA; reverse: GCGTCTCATGTGTCCCATTTG) BACE (sense: AGTCATCCACGGGCACTGTT; reverse: CTGAACTCATCGTGCACATGG), PSEN1 (sense: CTATAGCTCCCATGGCACCC; reverse: CTGAACCCGCCATCATCATT), Fe65 (sense: GAGAGTGTCGGGTGCGTTTC; reverse: TGAATGCAAACGTGTGGACAT) Tip60 (sense: TGAGGACTCCCAGGACAGCT; reverse: TCGTGGCTTCGATCAGACAC) Hes1 (sense: ACGTGCGAGGGCGTTAATAC; reverse: CATGGCATTGATCTGGGTCA) citrine-AICD (sense: CACTCTCGGCATGGACGAG; reverse: CGTCAACCTCCACCACACC). Real-time-PCR was performed with an ABI PRISM 7700 Sequence Detector (Applied Biosystems, Rotkreuz, Switzerland). The cycling conditions comprised a 2 minute pre-PCR at 50°C, 10 minutes polymerase activation at 95°C and 40 cycles at 95°C for 15 seconds and 60°C for 60 seconds. Sequence Detection Software (version 1.9.1) (Applied Biosystems, Rotkreuz, Switzerland) was used for data analyses.

Results

Localization of AFT-complexes to nuclear spots

An experimental difficulty in monitoring the subcellular trafficking of AICD is associated with its rapid degradation after γ-secretase cleavage (Cupers et al., 2001a; Kimberly et al., 2001). To overcome this difficulty, we constructed ecdyson-inducible expression vectors (Suhr et al., 1998) to express citrine-AICD fusion proteins comprising the 50 C-terminal residues of S3-cleaved APP. The fusion of citrine to the N-terminus of AICD may alter its properties; specifically we observed that citrine stabilizes the normally rapidly degraded AICD. The inducible expression vectors were flanked by inverted repeats for stable transfection with the sleeping beauty transposase system (Ivics et al., 1997). After inducing the expression of AICD with the ecdyson analogue tebufenozide in three isolated clonal lines identified by fluorescent microscopy, we found no evidence for degradation of the fusion protein on western blots (data not shown). Citrine fluorescence detected in the microscope therefore tracks the subcellular localization of the expressed AICD. Confocal analyses showed that AICD was localized homogenously in both cytosolic and nuclear compartments (Fig. 1A). The effect of APP-interacting proteins on AICD localization was analyzed with a Fe65 isoform containing the mini-exon 9, which has been shown to be expressed exclusively in neuronal cells (Hu et al., 1999). When we co-expressed AICD with Fe65 the two proteins localized both in cytosolic and nuclear compartments (Fig. 1B). Fe65 was described to be localized predominantly in nuclei in COS and H4 cells (Kimberly et al., 2001; Kinoshita et al., 2002; Minopoli et al., 2001). In HEK293 cells, nuclear accumulation was only seen after blockade of nuclear export (Fig. 3). Tip60 is a histone acetylase involved in many transcriptional signals via the modification of chromatin (Brady et al., 1999; Gaughan et al., 2001; Sterner and Berger, 2000). In the absence of Fe65, the CFP-Tip60 fusion protein was localized in nuclear structures with a speckle-like appearance (mean number=16.1, s.d.=6.8, median=14, n=29 cells, Fig. 1C). This localization of Tip60 had no effects whatsoever on the cellular distribution of AICD (Fig. 1D), suggesting that AICD did not bind to Tip60 in the absence of Fe65. By contrast, co-expression of Fe65 clearly resulted in binding to Tip60, and colocalization within circumscribed nuclear spots (Fig. 1E) with a distinct spherical geometry, clearly differing from the speckle-like morphology of the structures that included Tip60 alone. Expression of AICD in cells that co-expressed Fe65 together with Tip60 revealed a striking colocalization of AICD with Fe65 and Tip60 (AFT-complex) in these spherical nuclear spots, together with a drop in cytosolic AICD levels (Fig. 1F). This was observed consistently in virtually every cell co-expressing all three proteins (Fig. 1G). The mean diameter of AFT-complexes was 0.70 μm (s.d.=0.24, n=48 spots) and for Tip60 expressed alone the minimal diameter averaged at 1.77 μm (s.d.=0.45, n=49 spots). On average, we observed 32.0 nuclear spots with AFT-complexes (s.d.=20.8, median=25, n=32 cells). Mutation of the NKSY sequence of Tip60 to NASA, shown to prevent AICD-mediated transactivation in the Gal4 system (Cao and Südhof, 2001), still resulted in binding of Fe65-AICD-complexes to nuclear Tip60, but the formation of spherical spots was completely prevented (Fig. 1H). By contrast, the AFT-complexes formed with NASA-Tip60 had a speckle-like morphology. The change from spots to speckle-like morphology of AFT-complexes may be associated with the known functional changes of the Tip60 NASA mutation (Cao and Südhof, 2001).

Molecular association of AICD with the histone acetylase Tip60 in the presence of Fe65

To verify the molecular association of Tip60 and AICD in the AFT-complex, we performed fluorescence resonance energy transfer (FRET) measurements in cells with nuclear AICD-spots. We followed described FRET protocols (Gordon et al., 1998; Xia and Liu, 2001) to calculate the sensitized emission

of citrine-AICD after excitation of CFP-Tip60 (Fig. 2A). FRET was measured in 172 nuclear spots in 16 different nuclei, and an average NFRET value of 0.322 (s.d.=0.181) was calculated.

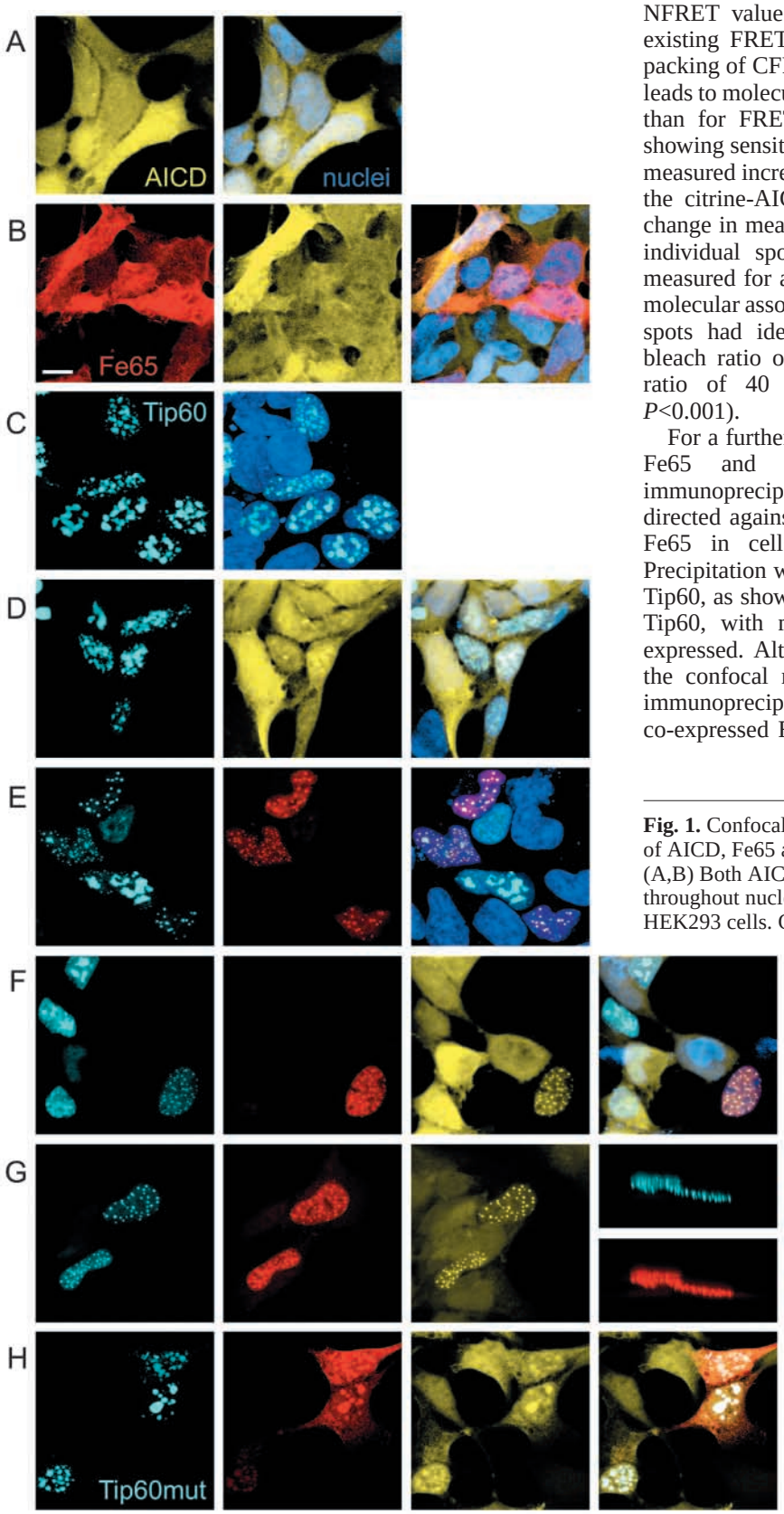

The co-expression of CFP and citrine tagged with a nuclear localization sequence resulted in strong nuclear signals from both fluorophores, but only a marginal FRET signal (Fig. 2B) (Average NFRET=0.066, s.d.=0.012, *n*=9 nuclei). This NFRET value is higher than described for values with no existing FRET (Xia and Liu, 2001), probably due to dense packing of CFP and citrine in the nuclear compartment, which leads to molecular encounters; however, it is still fivefold lower than for FRET from CFP-Tip60 to citrine-AICD. In cells showing sensitized emission of citrine-AICD (Fig. 2C) we also measured increased CFP-Tip60 fluorescence after bleaching of the citrine-AICD acceptor (Fig. 2D). The graphs show the change in mean CFP-fluorescence from pre- to post-bleach in individual spots. Unquenching of donor fluorescence was measured for all bleached nuclear spots, confirming the close molecular association of Tip60 and AICD, whereas unbleached spots had identical or diminished fluorescence (post-/pre-bleach ratio of 38 bleached spots: mean=1.114, s.d.=0.036; ratio of 40 unbleached spots: 1.001, s.d.=0.032; t-test $P<0.001$).

For a further support of the molecular interaction of AICD, Fe65 and Tip60 in the nucleus, we performed immunoprecipitations from nuclear fractions. Antibodies directed against both AICD and Tip60 are able to pull down Fe65 in cells expressing all three proteins (Fig. 2E). Precipitation with an antibody against AICD also enriches for Tip60, as shown by an antibody recognizing the CFP fused to Tip60, with more Tip60 pulled down when Fe65 is co-expressed. Although nuclear citrine-AICD can be imaged in the confocal microscope (Fig. 1A) it is not detectable by immunoprecipitation from nuclear fractions in the absence of co-expressed Fe65. Expression of Fe65, together with Tip60

Fig. 1. Confocal sections through nuclei show that AFT-complexes of AICD, Fe65 and Tip60 are localized to spherical nuclear spots. (A,B) Both AICD (yellow) and Fe65 (red) localized homogenously throughout nuclear (blue) and cytosolic compartments in transfected HEK293 cells. Co-expression of Fe65 and AICD resulted in the same localization. (C) In the absence of AICD and Fe65 co-expression, the histone acetylase Tip60 (cyan) localized to speckle-like nuclear structures. (D) In the absence of Fe65 co-expression, Tip60 had no effect on AICD distribution. (E) In the absence of AICD, Fe65 colocalized with Tip60 in nuclei and reorganized the speckle-like morphology into spherical nuclear spots. (F,G) In cells co-expressing AICD, Fe65 and Tip60, AICD was relocalized from the cytosol into AFT-complexes predominantly found in spherical nuclear spots. AFT-complexes were found throughout nuclei in all cells co-expressing the three proteins. Confocal xz sections of the same nuclei confirmed nuclear localization. (H) The NASA mutant of the putative Fe65-binding motif NKSY in Tip60 ineffectively localized some Fe65 and AICD to speckle-like nuclear structures, but completely abolished the formation of spherical nuclear spots. Bar, 10 μm.

leads to depletion of AICD from the cytosol and accumulation in nuclear spots (Fig. 1E,F), resulting in much higher nuclear levels of AICD, now detectable by immunoprecipitation. Alternatively, it is possible that free nuclear AICD, as seen in Fig. 1A, diffuses out of the nuclei during the preparation of nuclear fractions. AICD bound to a Tip60/Fe65-containing complex, which might be associated with chromatin, would not be washed away during the purification of nuclear fractions. After precipitation with antibodies against Tip60, the GFP antibodies also detect the citrine-AICD fusion protein, again only when Fe65 is cotransformed. The lower band in Fig. 2E, panel 4, is unspecific, resulting from the detection of the antibody used for immunoprecipitation by the secondary antibody used in western blots.

Active nuclear export of Fe65 is consistent with a function as a shuttle for AICD

To determine if Fe65 was actively cycling between nuclei and the cytosol, we blocked nuclear export by leptomycin B (Ni et al., 2001). After 9 hours of blocked export, Fe65 accumulated in nuclei (Fig. 3A). We measured the mean fluorescence intensity of nuclear and extranuclear compartments, as determined by DRAQ5 staining, after 24 hours of leptomycin B treatment. In control cells, the ratio of nuclear to extranuclear intensity measured in single confocal sections was 1.20

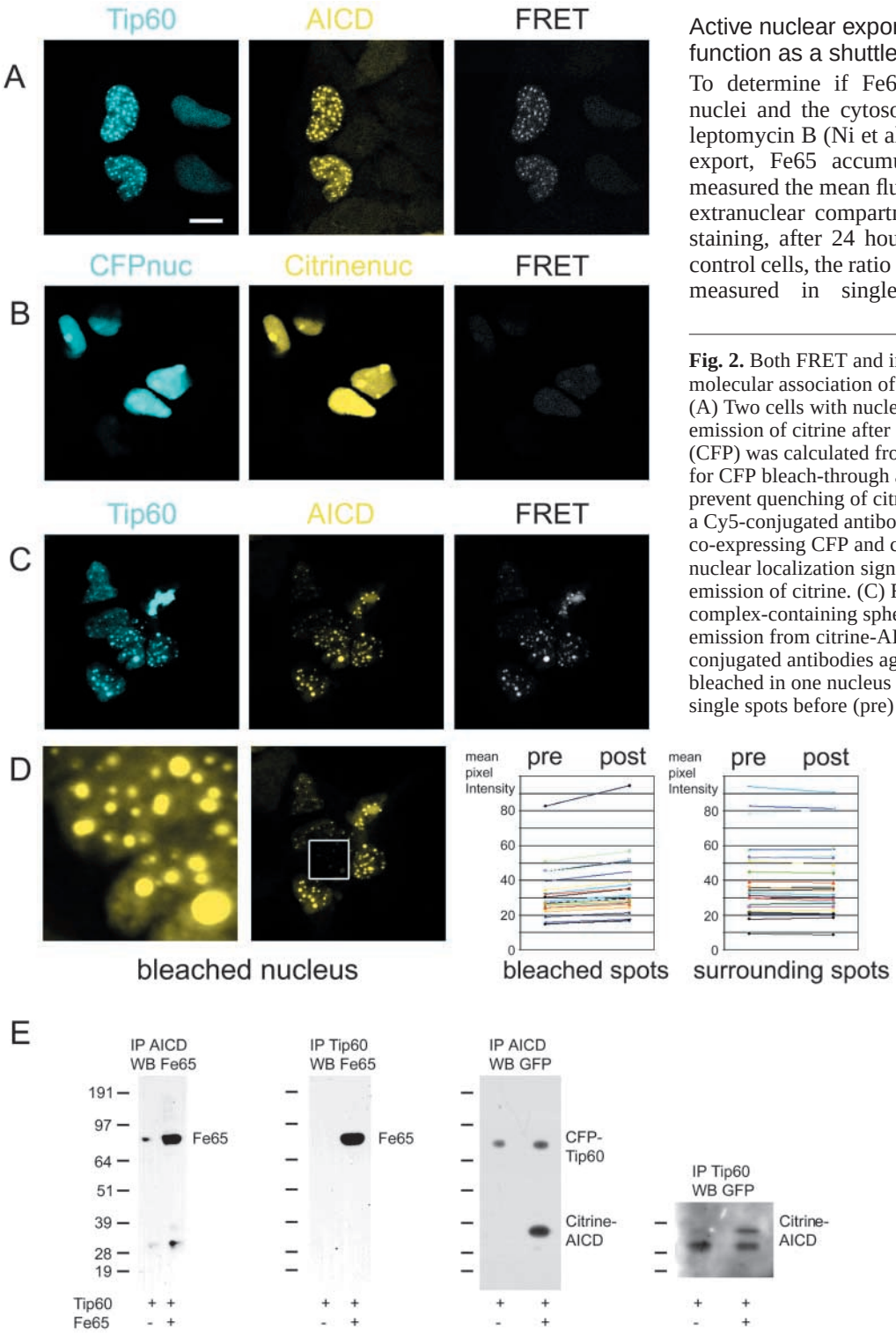

Fig. 2. Both FRET and immunoprecipitation reveal a close molecular association of Tip60 and AICD in AFT-complexes. (A) Two cells with nuclear AFT-complexes. Sensitized emission of citrine after excitation of cyan fluorescent protein (CFP) was calculated from raw FRET values with correction for CFP bleach-through and citrine cross-excitation. To prevent quenching of citrine emission, Fe65 was labeled with a Cy5-conjugated antibody (data not shown). (B) Control cells co-expressing CFP and citrine targeted to the nucleus with nuclear localization signals showed very little sensitized emission of citrine. (C) FRET measurements of AFT-complex-containing spherical nuclear spots showed sensitized emission from citrine-AICD in the absence of the Cy5-conjugated antibodies against Fe65. (D) Citrine-AICD was bleached in one nucleus and the intensity of CFP measured in single spots before (pre) and after bleaching (post). The graphs show the mean pixel intensity of the measured CFP-fluorescence. The pre/post values of single spots are connected by a line. After bleaching, CFP fluorescence intensities increased in spots in the bleached nucleus, but not in surrounding spots in unbleached nuclei. Bar, 10 μm. (E) Immunoprecipitation (IP) of AFT-complex components from nuclear fractions. Antibodies against AICD or Tip60 co-precipitate Fe65 as detected by western blot (WB) of the HA tag. IP with antibodies against AICD precipitated Tip60 and, vice versa, antibodies against Tip60 precipitated AICD, as shown by staining with an antibody against fluorescent proteins that detects both CFP and citrine. The lower band in panel 4 is unspecific, and results from the detection of the antibody used for immunoprecipitation by the secondary antibody used in western blots. Marker proteins are 19, 28, 39, 51, 64, 97 and 191 kDa.

(s.e.m.=0.06, *n*=35 cells). Leptomycin B treatment increased this ratio to 2.65 after 24 hours (s.e.m.=0.30, *n*=35 cells, t-test $P<0.001$, Fig. 3B). A similar increase was found for AICD, which changed from a nuclear/extranuclear intensity ratio of 0.76 (s.e.m.=0.04, *n*=35 cells) to 1.84 (s.e.m.=0.29, *n*=35 cells). In most of the Fe65-expressing cells we also observed the accumulation of AICD in nuclear spots after the inhibition of nuclear export (Fig. 3A), an observation we never made in cells co-expressing AICD and Fe65, and with intact nuclear export. In cells showing nuclear AICD spots we did not

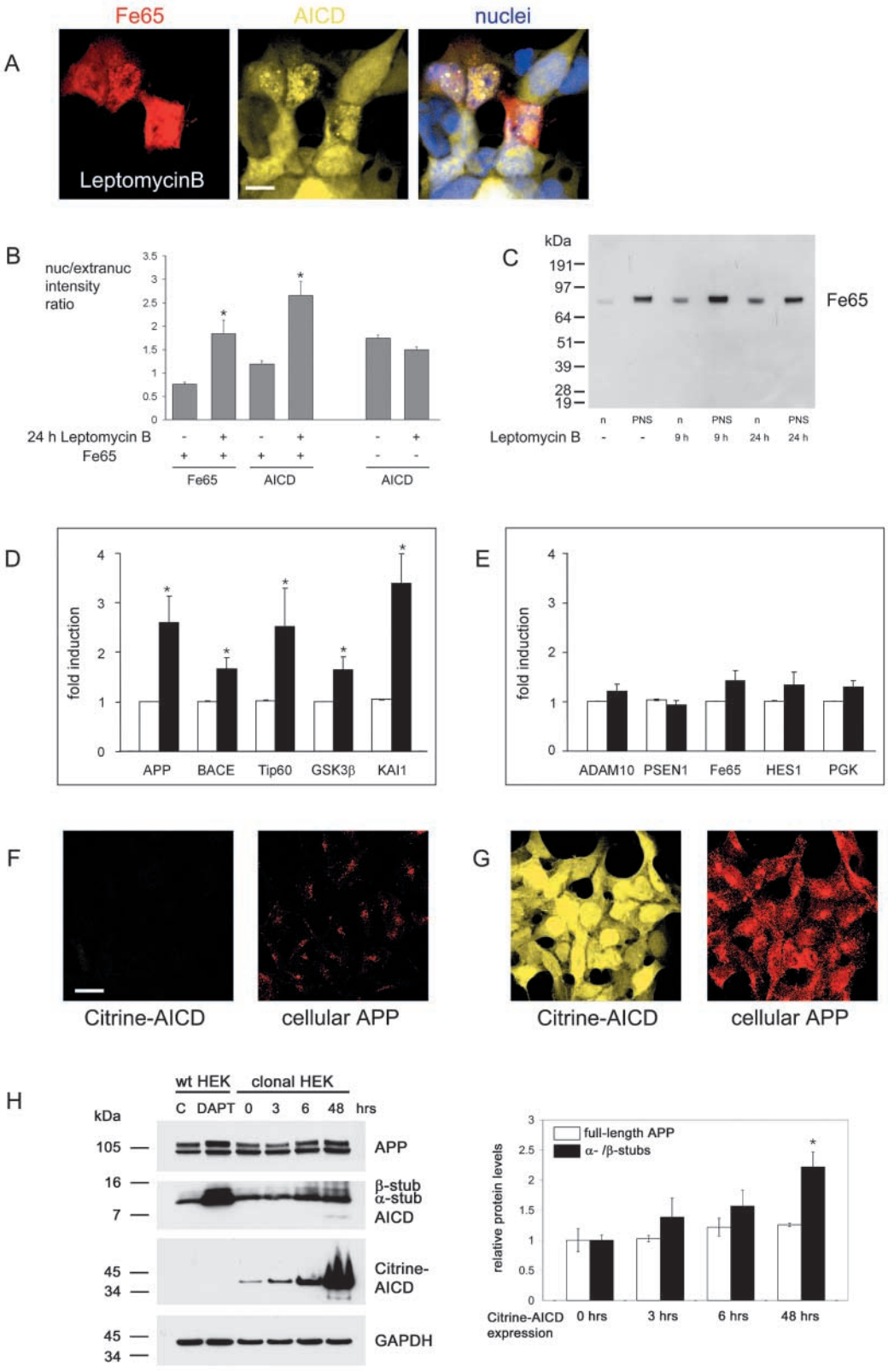

observe Fe65 enriched in these spots. This could be due to the general distribution of Fe65 in the nucleus, leading to less distinct labeling of spots. In addition, Fe65 is detected by antibody staining, which might differ in the multiprotein-complex-containing spots, whereas AICD is directly detected via the fused fluorescent protein. Cells expressing only AICD and treated with leptomycin B had no significant change in the ratio of nuclear-to-extranuclear intensity (control=1.74, s.e.m.=0.06; 24 hours leptomycin B=1.50, s.e.m.=0.05, n=35 cells each, Fig. 3B). Furthermore, we never observed nuclear AICD-spots after leptomycin B treatment in the absence of Fe65 co-expression.

We further treated cells co-expressing AICD and Fe65 with leptomycin B for 9 or 24 hours and prepared nuclear and postnuclear supernatant (PNS) fractions. Western blot analysis of Fe65 (Fig. 3C) again showed an increasing nuclear/PNS ratio with increasing time of inhibited nuclear export. Compared with intact nuclear export, the nuclear/PNS ratio increased to 247% after 9 hours and to 527% after 24 hours of leptomycin B treatment.

Regulation of AICD-effector genes

We isolated RNA populations from clonal cells with or without 48 hours of AICD induction. To determine whether inducible expression of AICD actually results in the regulation of the transcription of target genes, we performed real-time PCR experiments with genes coding for proteins involved in APP processing (*ADAM10, BACE, PSEN1*) or signaling (*Fe65, Tip60*). In addition, we analyzed the expression of *KAI1* and *GSK3β*, described candidate target genes of AICD (Baek et al., 2002; Kim et al., 2003). The increase in citrine-AICD transcripts after 48 hours of induction was 17.4 fold (range=±3.2, data not shown). We detected significantly increased transcript levels for *APP, BACE* and *Tip60*, as well as confirmed the regulation of *KAI1* and *GSK3β*, 48 hours after the induction of AICD expression (Mann-Whitney U, P<0.05, Fig. 3D). *ADAM10, PSEN1* and *Fe65* showed no regulation by AICD (Fig. 3E). The induction of AICD did not affect the expression of *Hes1*, a Notch-effector gene regulated by NICD (Ohtsuka et al., 1999). Normalizations were performed with *GAPDH* and *PGK*, yielding similar results. To judge variation, *PGK* is also plotted against *GAPDH*.

The fact that AICD regulates the transcription of its precursor prompted us to test whether protein levels of APP are also upregulated. We induced AICD-citrine expression for 48 hours in clonal HEK293 lines. Staining with antibody 6E10, which stains the Aβ-domain of endogenous APP and thus detects sAPPα, Aβ and β-stubs besides full-length APP, was performed identically on uninduced cells to determine baseline expression. Confocal images, acquired with identical instrument settings, showed a strong increase in cellular APP levels (Fig. 3F,G). Therefore, AICD induces not only the transcription of *APP* but also results in increased protein levels. We next analyzed APP expression with western blots of wild-type HEK293 and clonal lines with different induction times of AICD expression (Fig. 3H). There was no significant increase in the levels of full-length APP at 3, 6 and 48 hours of AICD expression, compared with uninduced cells (normalized to GAPDH). By contrast, we detected increases in α- and β-stubs, reaching 2.2-fold (s.e.m.=0.2, n=3) of the levels seen in uninduced cells after 48 hours of induction of citrine-AICD expression (Mann-Whitney U, P<0.05, Fig. 3H). Furthermore, after 48 hours of expression of citrine-AICD we could detect endogenous AICD in addition to α- and β-stubs. The increase in α- and β-stubs was also seen in naive HEK293 cells after inhibition of γ-secretase with DAPT. Compared with naive HEK293 we could detect nearly twofold higher levels of full-length APP and stubs in uninduced AICD-expressing cell lines. This might be due to leakage of AICD expression with our inducible system, which is not evident via confocal microscopy (Fig. 3F) but can be detected in western blots (Fig. 3H).

Fig. 3. Fe65 transports AICD to nuclei where it can regulate transcription. (A) Blocking nuclear export with leptomycin B for 9 hours leads to an accumulation of Fe65 and AICD in nuclei. In cells co-expressing Fe65 and AICD, leptomycin B caused the formation of nuclear AICD-containing spots that were never observed in cells without the cotransfection of Fe65, or in the absence of leptomycin B (compare Fig. 1A,B). Bar, 10 μm. (B) Leptomycin B (24 hours) increased fluorescence signal intensity ratios of nuclear versus extranuclear staining for AICD and Fe65 in co-expressing cells. Without the expression of Fe65, leptomycin B treatment did not change the nuclear/extranuclear signal ratio for AICD. (C) Western blots of nuclear (n) and post-nuclear supernatant (PNS) fractions from AICD- and Fe65-expressing cells treated with lepomycin B (0 to 24 hours) showed increased nuclear retention of Fe65. The nuclear/PNS signal ratio for Fe65 increased to 247% after 9 hours and to 527% after 24 hours, as compared with a 100% baseline. Marker proteins are 19, 28, 39, 51, 64, 97 and 191 kDa. (D,E) Real-time PCR of clonal cell lines with and without the induced expression of citrine-AICD revealed that AICD increased the expression of *APP, BACE* and *Tip60* (Mann-Whitney U, P<0.05). AICD did not change the expression of *Fe65, Tip60, ADAM10, PSEN1*, or the Notch-effector gene *Hes1*. The AICD-induced expression of *KAI1* and *Gsk3β* was confirmed. All values were normalized against GAPDH expression levels and expressed as fold baseline without induction of AICD expression. Data represent means ± s.e.m. of five experiments, each done in triplicate. (F,G) Clonal HEK293 grown for 48 hours without (F) or with (G) the induction of AICD-citrine expression. 6E10-staining for endogenous APP reveals increased protein levels induced by AICD. Bar, 20 μm. (H) Whole cell extracts of naive HEK293 and AICD-expressing clonal cell lines. Western blots were analyzed with antibodies against the N- or C-terminus of APP, against GFP to detect the citrine-AICD fusion protein and GAPDH as a loading control. Naive HEK293 (C, lane 1) were also treated with the γ-secretase inhibitor DAPT, which leads to accumulation of α- and β-stubs (DAPT, lane 2). Clonal HEK293 were induced for 3, 6 or 48 hours (lane 4 to 6) to express citrine-AICD. Bar diagram shows densitometric analysis of full-length APP and α- together with β-stubs from three independent experiments. Relative protein levels are determined with respect to uninduced cells (0 hrs).

Jip1 targets AICD to Tip60 whereas X11 traps it to extranuclear sites

The jun-interacting protein (Jip1) is another APP-adaptor protein (Matsuda et al., 2001; Scheinfeld et al., 2002b; Taru et al., 2002a; Taru et al., 2002b) that shows transactivation activity in the Gal4 system (Scheinfeld et al., 2003). Jip1b is a splice variant with an insertion of 47 amino acids in the COOH-terminal phosphotyrosine binding (PTB) domain of Jip1 (Whitmarsh et al., 1998). Transfection of Jip1b into AICD-expressing cells reveals an extranuclear localization.

Binding of AICD by Jip1b is evident from the clearance of AICD from the nucleus (Fig. 4A). Surprisingly, when Tip60 is co-expressed Jip1b localizes to nuclear speckles (Fig. 4B). In contrast to Fe65, the speckles show the same morphology as Tip60 alone. AICD is also localized to these speckles, although at lower levels than seen with Fe65, and AICD is still detected in the cytosol (Fig. 4C). The number of speckles per nucleus was 10.7 (s.d.=5.1, median=10, *n*=63 nuclei), which was significantly lower than spot numbers with Fe65-containing complexes. From our data we cannot determine whether the interaction between Tip60 and Jip1b is direct or indirect via the recruitment of additional endogenous proteins. When Jip1b was transformed together with the functionally impaired, NASA-mutated Tip60 (Cao and Südhof, 2001) it still localized together with Tip60 in speckle-like structures (not shown).

Cotransformation of X11α (MINT1), another APP-adaptor protein (Borg et al., 1996), showed a subcellular distribution similar to Jip1b, with no signal detected in the nucleus. Again, the binding of AICD to X11α led to a clearance of AICD from the nucleus (Fig. 4D). X11α has an inhibitory effect on AICD-mediated transactivation in the Gal4 system (Biederer et al., 2002). Tip60 did not relocate X11α to nuclear spots and no nuclear AICD was detectable (Fig. 4E). X11α thus traps AICD in the cytosol and therefore differs from the effects of Fe65 and Jip1b on nuclear AICD localization.

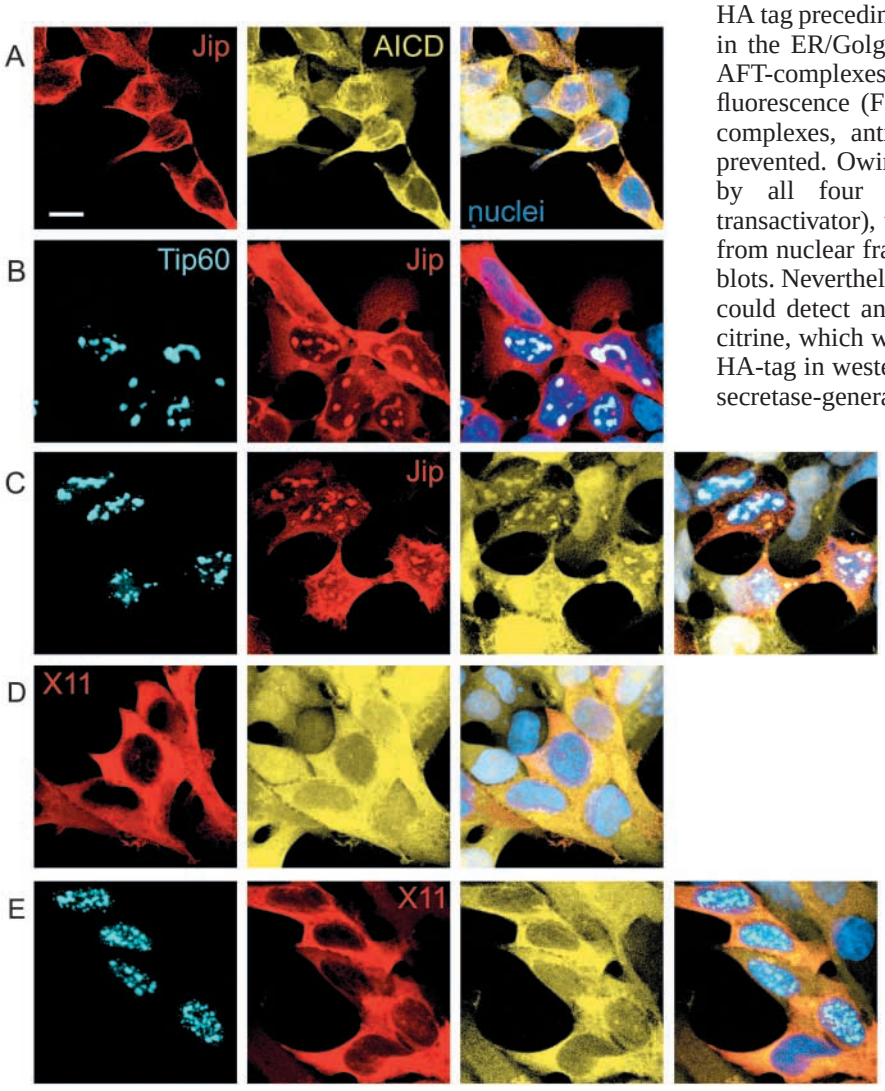

Fig. 4. APP-interacting proteins Jip1b and X11α have different effects on nuclear AICD localization. (A) Extranuclear localization of Jip1b. Binding of AICD to Jip1b was associated with decreased nuclear levels of AICD. (B) Co-expression of Tip60 relocalized Jip1b into nuclear speckles. (C) Additional co-expression of AICD resulted in the formation of nuclear AICD-Jip1-Tip60 (AJT) complexes with a distinct speckle-like morphology, as compared with the smaller spherical spots generated by AFT-complexes. (D) Exclusive extranuclear localization of X11α. Binding of AICD to X11α was associated with decreased nuclear levels of AICD. (E) Co-expression of Tip60 had no effect on the extranuclear localization of either X11α or AICD. Bar, 10 μm.

Full-length APP-derived AICD translocates to nuclei – inhibition by γ-secretase inhibitors

To verify whether AICD generated from full-length APP also translocates to the nucleus we expressed APP_{695}-citrine fusion proteins via the ecdyson-inducible system. The citrine cDNA was cloned downstream of the C-terminus of APP, either via a short spacer or a longer spacer coding for a tandem HA tag (see Materials and Methods). Sixteen hours after the induction of transgene expression citrine fluorescence was detected in the perinuclear endoplasmic reticulum and the Golgi complex, and highly colocalized with the HA tag staining (Fig. 5A). Furthermore, APP-fluorescence was seen in spots covering the membrane surface of the soma and all processes. This pattern resembled the distribution of endogenous APP. No fluorescence was detected in the nucleus when observing confocal sections. Cotransformation of Fe65 and Tip60 again led to the appearance of AICD-citrine fluorescence in nuclear spots (Fig. 5B). One APP-citrine construct contained a tandem HA tag preceding the citrine. The HA tag antibody stained APP in the ER/Golgi and processes, but it failed to label nuclear AFT-complexes, which were readily detected via the citrine fluorescence (Fig. 5C). With the formation of nuclear AFT-complexes, antibody access to the HA tag was obviously prevented. Owing to the low percentage of cells transformed by all four constructs (APP, Fe65, Tip60, ecdysone transactivator), we were not able to immunoprecipitate AICD from nuclear fractions and test for HA tag staining in western blots. Nevertheless, using homogenates of transfected cells, we could detect an approximately 35 kDa band of AICD-2HA-citrine, which was detected by antibodies against GFP and the HA-tag in western blots (data not shown). The integrity of the secretase-generated AICD-HA tag-citrine fusion protein can be

inferred from the fact that citrine alone was not targeted to nuclear spots containing Fe65 and Tip60 (data not shown). As the AICD sequence is responsible for localization to nuclear spots where citrine fluorescence is observable, the connecting HA tag must be intact. Fig. 5D shows another cell with the HA tag of APP stained with Cy5 to enable FRET measurements. Again, the HA tag-staining detected APP in the soma and processes, but failed to label nuclear AFT-complexes. Excitation of CFP-Tip60 resulted in sensitized emission from APP-derived AICD-citrine, localized in nuclear spherical spots. Together with the failure of anti-HA antibody staining of nuclear spots, this shows the close molecular interaction in AFT-complexes.

Sequential cleavage of transmembrane APP by secretases liberates AICD from the membrane. Inhibition of γ-secretase by L-685,458 (Shearman et al., 2000) or DAPT (Geling et al., 2002; Sastre et al., 2001) completely abolished the formation of nuclear AICD spots from APP-citrine fusion proteins. None of the cells co-expressing APP, Fe65 and Tip60 showed nuclear AICD localization (*n*=15 cells with L-685,458, *n*=27 cells with DAPT). In cells with low-to-medium levels of APP expression Fe65 localized to spherical nuclear spots together with Tip60 (*n*=25 cells), despite the inhibition of nuclear AICD localization (Fig. 6A, upper cell and 6B). The nuclear localization of Fe65 was prevented in cells with high APP expression (*n*=17 cells) (Fig. 6A, lower cell); instead it closely resembled the distribution of APP. Without the inhibition of γ-secretase the formation of nuclear spots with spherical AFT-complexes was seen in 69 out of 76 cells expressing all three proteins (Fig. 6C).

Formation of nuclear AFT- and AJT-complexes in differentiated neuroblastoma cells

Transient transfections were also done in SH-SY5Y cells differentiated for 10 days with retinoic acid and BDNF. In these cells Fe65 was already concentrated in the nucleus without the addition of Tip60 (Fig. 7A). Co-expression of AICD, Fe65 and Tip60 again led to the formation of spherical nuclear spots of AFT-complexes (Fig. 7B). As seen in HEK293 cells, Jip1b and X11α had an extranuclear localization leading to a similar localization of AICD. Co-expression of Tip60 resulted in the relocalization of Jip1 and AICD to nuclear AJT-complexes, with speckle-like morphology (Fig. 7C). Finally, co-expression of full-length APP with Fe65 and Tip60 also resulted in the appearance of AICD in nuclear spots (Fig. 7D). Thus, cells differentiated into a neuronal phenotype also show the formation of AFT- and AJT-complexes in the nuclear compartment.

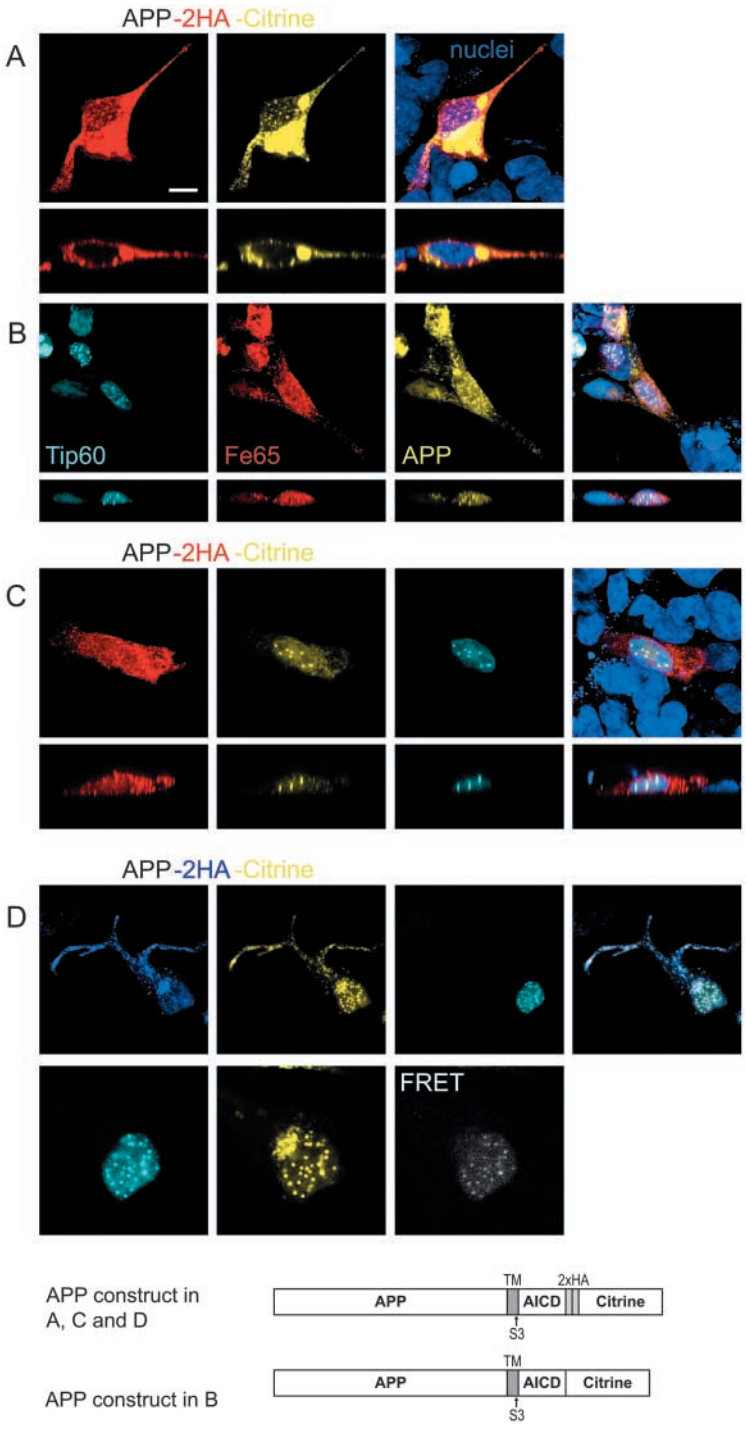

Fig. 5. AICD derived from full-length APP translocates to the nucleus and generates AFT-complexes. (A) Cells expressing APP fused to a C-terminal HA tag (red) followed in tandem by citrine (yellow). As expected, full-length APP was localized in the ER/Golgi and in vesicles in the processes and somata, but not in nuclei. Staining of APP with antibodies directed against the C-terminal HA tag colocalized with citrine fluorescence in extranuclear localizations. Confocal xz-scans through nuclei confirmed the extranuclear localization of full-length APP. (B) Cells co-expressing full-length APP together with Fe65 and Tip60 formed nuclear AFT-complexes with spherical spot morphology. (C) In contrast to the extranuclear colocalization of HA antibody staining with citrine fluorescence, HA antibodies failed to detect the nuclear AFT-complexes that emitted strong citrine fluorescence signals. (D) FRET measurements showed close molecular association of APP-derived AICD with Tip60 in nuclear AFT-complexes. Antibodies against the C-terminal HA tag of APP, stained with Cy5 (blue), consistently failed to detect AICD in AFT-complexes. Bar, 10 μm in A to C, 20 μm in D upper row and 5 μm in D lower row.

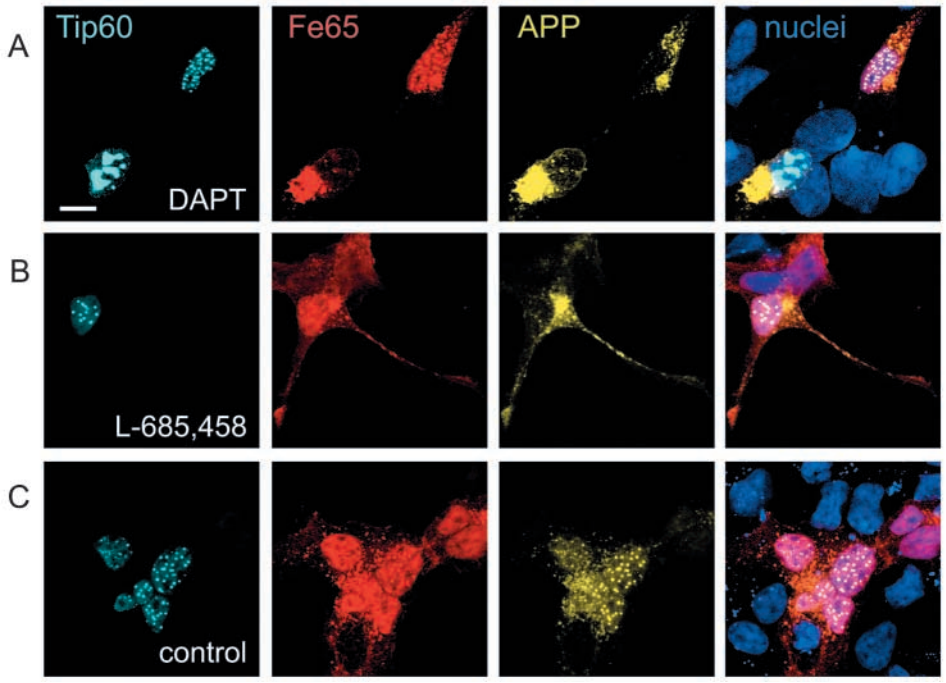

Fig. 6. Pharmacological inhibition of γ-secretase processing of APP blocks the formation of nuclear AFT-complexes. (A,B) The γ-secretase inhibitors DAPT and L-685,458 prevented the localization of APP-derived AICD into nuclear AFT-complexes. In cells with lower APP expression Fe65 was targeted to nuclear spots, whereas in cells with high levels of APP, Fe65 was retained at extranuclear localizations of APP including the ER/Golgi and vesicular structures. (C) Control experiment in the absence of γ-secretase inhibitors confirmed the formation of APP-derived nuclear AFT-complexes. Bar, 10 μm.

Discussion

The results of this study show that the APP-binding adaptor proteins Fe65, Jip1b and X11α (MINT1) differentially regulate the formation of nuclear AICD-containing complexes. Our data also establish that AICD increased the transcription of the AICD-effector genes *APP*, *BACE* and *Tip60*, in addition to *GSK3β* and *KAI1*.

Regulation of nuclear AICD targeting

To characterize the cellular trafficking of the APP-derived AICD generated by γ-secretase, we expressed citrine-AICD fusion proteins representing the S3-cleaved APP C-terminus by using an ecdyson-inducible expression system. Co-expression of AICD-adaptor proteins showed that Fe65 or Jip1b targeted the AICD to specific nuclear loci, whereas X11α trapped it in the cytosol. Blocking nuclear export showed that Fe65 is actively cycled between nuclear and cytosolic compartments and can transport bound AICD. Within nuclei Fe65 or Jip1b docked with bound AICD to the histone acetylase Tip60 and formed AICD-containing AFT- or AJT-complexes with clearly distinctive morphologies. Nuclear AFT-complexes appeared in multiple homogenous spherical spots, whereas AJT-complexes occupied a significantly lower number of speckle-like structures. The different morphology of the spherical spots containing AFT-complexes compared with the speckle-like structures containing the AJT-complexes suggests that they might involve the regulation of different sets of genes associated with different cellular functions. The precise functions of AFT- and AJT-complexes are unknown, but our measurements indicated that the nuclear structures containing these complexes are very large, consistent with the possibility that they contain additional proteins or DNA required for transcriptional activity. Both FRET and IP analyses illustrated the close molecular interaction of AICD with Tip60 in the nuclear complexes. Additional studies are required to determine whether they represent sites of active transcription.

The differential effects on nuclear targeting of AICD are consistent with data from yeast Gal4 transactivation experiments that showed transactivation activity for AICD together with either Fe65 or Jip1b, and inhibitory activities of X11α (Cao and Sudhof, 2001; Biederer et al., 2002; Scheinfeld et al., 2003). The nuclear translocation of intracellular domains liberated from membranes by γ-secretase is an emerging concept underscored by the fact that both Notch and N-cadherin use this pathway for signaling from the cell surface to the nucleus to regulate transcription (Schroeter et al., 1998; Marambaud et al., 2003).

Full-length APP functions in nuclear signaling

Our results show that the AICD generated from full-length APP by γ-cleavage at the plasma membrane (Cupers et al., 2001b) can be transported to the nucleus by Fe65, and docked onto Tip60 both in HEK293 and differentiated SH-SY5Y cells, suggesting the possibility that APP also functions in nuclear signaling in neuronal cells. Neurons express high endogenous levels of APP, Fe65 and Tip60 (Card et al., 1988; Hu et al., 1999; Ran and Pereira-Smith, 2000; Russo et al., 1998; Shivers et al., 1988), and neurons process APP to form AICD. It is therefore conceivable that neurons can form AFT- and AJT-complexes. Despite the fact that recent experiments claimed the presence of intranuclear AICD in neurons (Kimberly et al., 2001), many previous attempts to localize AICD immunohistochemically in nuclei of neuronal cells or brain tissue sections failed. The reasons for this absence of antibody staining could involve sensitivity issues, as well as the short half-life of free cytosolic AICD, but our results offer an alternative explanation. Our APP-derived AICD with a tandem HA-citrine tag allowed us to localize nuclear AICD via the

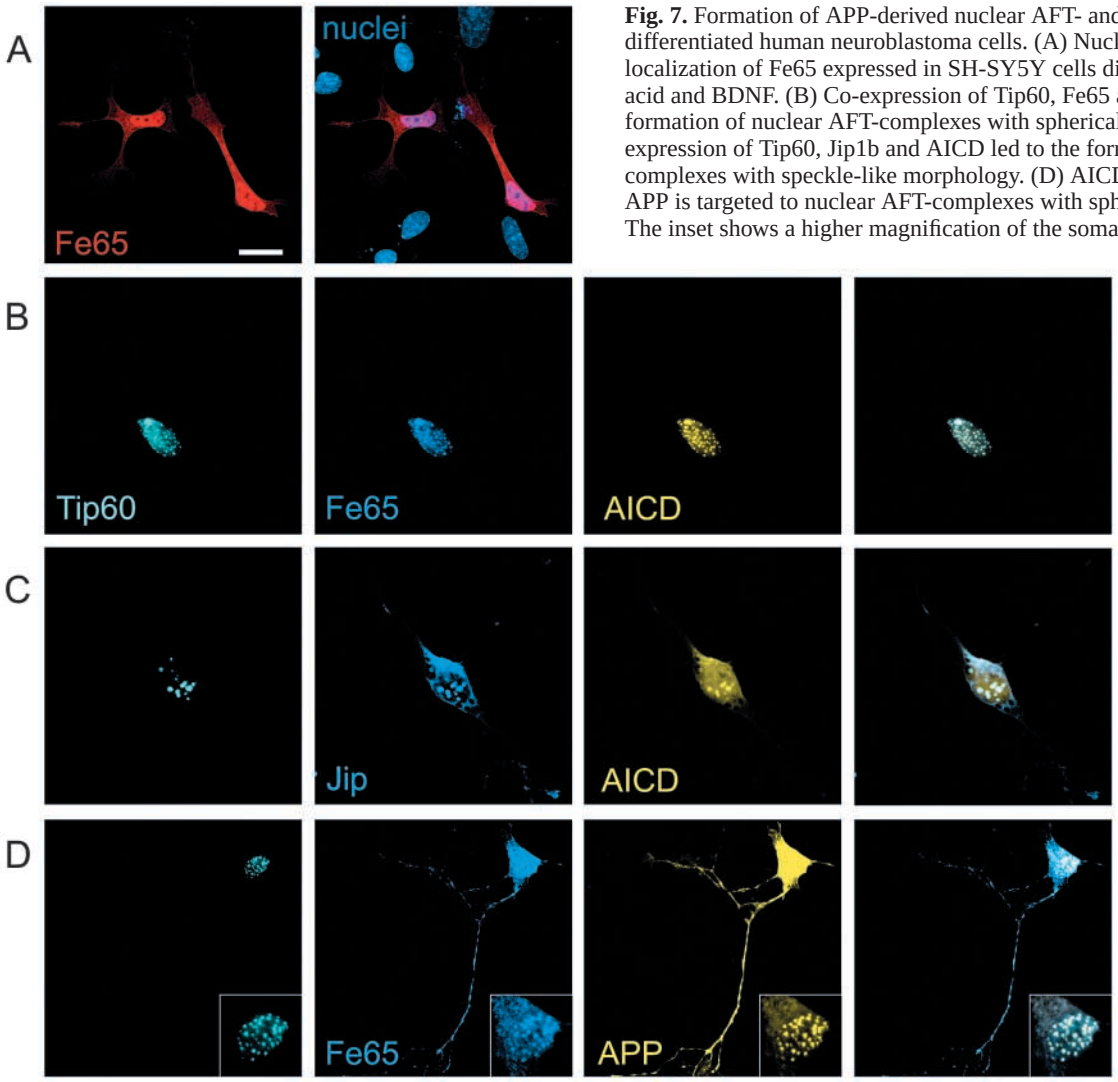

Fig. 7. Formation of APP-derived nuclear AFT- and AJT-complexes in differentiated human neuroblastoma cells. (A) Nuclear and cytoplasmic localization of Fe65 expressed in SH-SY5Y cells differentiated with retinoic acid and BDNF. (B) Co-expression of Tip60, Fe65 and AICD led to the formation of nuclear AFT-complexes with spherical spot morphology. (C) Co-expression of Tip60, Jip1b and AICD led to the formation of nuclear AJT-complexes with speckle-like morphology. (D) AICD derived from full-length APP is targeted to nuclear AFT-complexes with spherical spot morphology. The inset shows a higher magnification of the soma, with a lower exposure to visualize nuclear spots, which are over-exposed in the overview. Bar in A: 20 μm for A,D; 10 μm for B,C,D inset.

direct citrine fluorescence, while antibodies against the HA tag at the C-terminus clearly bound to AICD in the cytoplasm, but not to the nuclear AFT-complexes. These data suggest that nuclear complex formation with Tip60 and Fe65 prevents antibody access to AICD. Therefore, either more elaborate protocols for tissue permeabilization or transgenic approaches with fluorescent APP fusion proteins are required to show nuclear AICD complexes in vivo.

AICD-dependent regulation of gene expression

To test the hypothesis that AICD controls genes involved in the regulation of cellular levels of APP, we analyzed transcripts encoding APP upon induced expression of AICD. By using clonal cell lines with inducible expression constructs, we generated two mRNA populations differing only in the expression of AICD and its putative downstream effector genes. These experiments clearly showed that AICD upregulated the expression of the *APP* genes as part of a positive feedback mechanism, by which APP senses its own endoproteolysis and upregulates its expression to replenish full-length APP. We next tested the hypothesis that AICD regulates the expression of enzymes involved in its generation and established that AICD upregulates the gene encoding the β-site APP cleaving enzyme (*BACE*), but not the γ-secretase-complex protein *PSEN1* or *ADAM10*, one of the proposed α-secretases (Vassar et al., 1999; Edbauer et al., 2003; Lammich et al., 1999). To be functionally meaningful for nuclear signaling, this positive feedback amplification of AICD should be associated with increased levels of the components of the nuclear AFT-complex. Therefore, in the same cells we analyzed the expression of *Tip60* and *Fe65* and found that AICD also increased the expression of *Tip60*. These data could explain the recent observation of increased Tip60 in APP transgenic mice (Baek et al., 2002). In the same cell lines, we were able to confirm the previously reported AICD-dependent induction of *KAI-1* and *GSK3β* (Baek et al., 2002; Kim et al., 2003). Together, these results establish that APP not only regulates its own expression but also the expression of several genes involved in its processing and cellular function. Importantly, the NICD-effector gene *Hes1* of the Notch signaling pathway, which is also regulated by γ-secretase, was unaffected by AICD. From these data we cannot exclude the possibility that the effect of AICD on transcription is indirect,

i.e. by influencing the nuclear signaling of other pathways controlling transcription. Nevertheless, Cao and Südhof (Cao and Südhof, 2001) have shown a transcription-activating activity for AICD bound to Fe65, and we show the colocalization of AICD together with Fe65 and Tip60 in discrete nuclear spots. If the average number of 32 AFT-complex-containing nuclear spots and 11 AJT-complex-containing speckles are related to the number of AICD-regulated genes, it is probable that more than the above genes are regulated by APP signaling.

The increase in APP transcripts is accompanied by increased levels of protein. In particular, C-terminal stubs were significantly increased in parallel to the induced expression of AICD. The fact that steady-state levels of full-length APP did not increase significantly in this condition is probably related to the observed concomitant increase in BACE expression, which is expected to increase the turnover of full-length APP; a similar mechanism may be involved in the observed increased generation of α-stubs. Together, these data are consistent with the idea that the steady-state levels of APP are maintained at constant cellular concentrations under physiological conditions. The life cycle of APP therefore encompasses a feedback mechanism of synthesis, subcellular sorting, proteolytic cleavages and finally nuclear signaling and transcriptional activation of *APP* by AICD. The additional cellular effects of the AICD-induced increase in APP turnover remain to be determined.

Role of γ-secretase processing in nuclear signaling

The nuclear translocation of intracellular domains liberated from membranes by γ-secretase is an emerging concept for signaling from the cell surface to the nucleus, to regulate gene transcription. The intracellular domains cleaved from the membrane-bound precursors Notch, ErbB4, Neuregulin1, LRP, N-cadherin APLP1, APLP2 and APP translocate to nuclei, and transactivation activity was shown for Notch, Delta 1, Neuregulin1, N-cadherin, APLP1, APLP2 and APP (Bao et al., 2003; Ikeuchi and Sisodia, 2003; Kimberly et al., 2001; Kinoshita et al., 2002; Kinoshita et al., 2003; Marambaud et al., 2003; May et al., 2002; Ni et al., 2001; Scheinfeld et al., 2002a; Schroeter et al., 1998; Walsh et al., 2003). Besides the γ-secretase complex similar adaptor-proteins are involved in nuclear signaling; for example, LRP can bind Fe65 via a different phosphotyrosine-interacting domain than AICD (Kinoshita et al., 2001), and binding of numb by APP influences Notch signaling (Roncarati et al., 2002). Finally, in the nucleus the histone acetylase Tip60 is involved in chromatin remodeling for a variety of signals including STAT-3 (signal transducer and activator of transcription-3), CREB, c-myc, nuclear hormone receptors (Brady et al., 1999; Frank et al., 2003; Gaughan et al., 2001; Xiao et al., 2003). The LRP-ICD generated by γ-secretase cleavage was recently shown to also localize with Tip60 in nuclear speckles (Kinoshita et al., 2003). Together, these findings suggest that γ-secretase processing of membrane proteins is involved in multiple signaling pathways, and that cross-talk of these pathways by means of the common interaction partners could affect APP-dependent nuclear signaling. In addition, these observations suggest that AICD-regulated genes are a subset of a much larger group of genes controlled by γ-secretase processing.

In summary, our data provide strong evidence in favor of nuclear signaling functions of AICD and they show that these functions are regulated by the APP-adaptor proteins Fe65, Jip1b and X11α, as well as the nuclear docking protein Tip60. AICD regulates the expression of its precursor APP and therefore acts as a signal of APP cleavage, leading to the replenishment of full-length APP levels. In the light of these functions of AICD, and the growing list of γ-secretase-substrates that signal to the nucleus, the therapeutic use of γ-secretase inhibitors needs to be carefully evaluated.

We are grateful to Boris Zarda and Andreas Luethi from Leica for ongoing support with the confocal microscope. Special thanks to Jay Tracy for comments on the manuscript. The following people kindly supplied us with cDNA constructs: Steve Suhr (Bombyx mori expression system), Stefan Kins, Beyreuther lab (Fe65), Zoltan Ivics (sleeping beauty), Maria Alexander (GAPDH promotor), R.Y. Tsien (citrine) and Craig Robson (Tip60).

This work was supported in parts by the SFB (6027) on Structure and Function of Membrane Proteins, a career development grant from the University of Zurich to U.K., the NCCR on Neural Plasticity and Regeneration and the EU DIADEM program.

References

Alexander, M. C., Lomanto, M., Nasrin, N. and Ramaika, C. (1988). Insulin stimulates glyceraldehyde-3-phosphate dehydrogenase gene expression through cis-acting DNA sequences. *Proc. Natl. Acad. Sci. USA* **85**, 5092-5096.

Baek, S. H., Ohgi, K. A., Rose, D. W., Koo, E. H., Glass, C. K. and Rosenfeld, M. G. (2002). Exchange of N-CoR corepressor and Tip60 coactivator complexes links gene expression by NF-kappaB and beta-amyloid precursor protein. *Cell* **110**, 55-67.

Bao, J., Wolpowitz, D., Role, L. W. and Talmage, D. A. (2003). Back signaling by the Nrg-1 intracellular domain. *J. Cell Biol.* **161**, 1133-1141.

Biederer, T., Cao, X., Sudhof, T. C. and Liu, X. (2002). Regulation of APP-dependent transcription complexes by Mint/X11s: differential functions of Mint isoforms. *J. Neurosci.* **22**, 7340-7351.

Borg, J. P., Ooi, J., Levy, E. and Margolis, B. (1996). The phosphotyrosine interaction domains of X11 and FE65 bind to distinct sites on the YENPTY motif of amyloid precursor protein. *Mol. Cell. Biol.* **16**, 6229-6241.

Brady, M. E., Ozanne, D. M., Gaughan, L., Waite, I., Cook, S., Neal, D. E. and Robson, C. N. (1999). Tip60 is a nuclear hormone receptor coactivator. *J. Biol. Chem.* **274**, 17599-17604.

Cao, X. and Sudhof, T. C. (2001). A transcriptionally active complex of APP with Fe65 and histone acetyltransferase Tip60. *Science* **293**, 115-120.

Card, J. P., Meade, R. P. and Davis, L. G. (1988). Immunocytochemical localization of the precursor protein for beta-amyloid in the rat central nervous system. *Neuron* **1**, 835-846.

Cupers, P., Orlans, I., Craessaerts, K., Annaert, W. and de Strooper, B. (2001a). The amyloid precursor protein (APP)-cytoplasmic fragment generated by gamma-secretase is rapidly degraded but distributes partially in a nuclear fraction of neurones in culture. *J. Neurochem.* **78**, 1168-1178.

Cupers, P., Bentahir, M., Craessaerts, K., Orlans, I., Vanderstichele, H., Saftig, P., de Strooper, B. and Annaert, W. (2001b). The discrepancy between presenilin subcellular localization and gamma-secretase processing of amyloid precursor protein. *J. Cell Biol.* **154**, 731-740.

De Strooper, B. (2003). Aph-1, Pen-2, and nicastrin with presenilin generate an active gamma-secretase complex. *Neuron* **38**, 9-12.

De Strooper, B., Annaert, W., Cupers, P., Saftig, P., Craessaerts, K., Mumm, J. S., Schroeter, E. H., Schrijvers, V., Wolfe, M. S., Ray, W. J. et al. (1999). A presenilin-1-dependent gamma-secretase-like protease mediates release of Notch intracellular domain. *Nature* **398**, 518-522.

Duilio, A., Zambrano, N., Mogavero, A. R., Ammendola, R., Cimino, F. and Russo, T. (1991). A rat brain mRNA encoding a transcriptional activator homologous to the DNA binding domain of retroviral integrases. *Nucleic Acids Res.* **19**, 5269-5274.

Edbauer, D., Willem, M., Lammich, S., Steiner, H. and Haass, C. (2002).

Insulin-degrading enzyme rapidly removes the beta-amyloid precursor protein intracellular domain (AICD). *J. Biol. Chem.* **277**, 13389-13393.

Edbauer, D., Winkler, E., Regula, J. T., Pesold, B., Steiner, H. and Haass, C. (2003). Reconstitution of gamma-secretase activity. *Nat. Cell Biol.* **5**, 486-488.

Farris, W., Mansourian, S., Chang, Y., Lindsley, L., Eckman, E. A., Frosch, M. P., Eckman, C. B., Tanzi, R. E., Selkoe, D. J. and Guenette, S. (2003). Insulin-degrading enzyme regulates the levels of insulin, amyloid beta-protein, and the beta-amyloid precursor protein intracellular domain in vivo. *Proc. Natl. Acad. Sci. USA* **100**, 4162-4167.

Frank, S. R., Parisi, T., Taubert, S., Fernandez, P., Fuchs, M., Chan, H. M., Livingston, D. M. and Amati, B. (2003). MYC recruits the TIP60 histone acetyltransferase complex to chromatin. *EMBO Rep.* **4**, 575-580.

Gaughan, L., Brady, M. E., Cook, S., Neal, D. E. and Robson, C. N. (2001). Tip60 is a co-activator specific for class I nuclear hormone receptors. *J. Biol. Chem.* **276**, 46841-46848.

Geling, A., Steiner, H., Willem, M., Bally-Cuif, L. and Haass, C. (2002). A gamma-secretase inhibitor blocks Notch signaling in vivo and causes a severe neurogenic phenotype in zebrafish. *EMBO Rep.* **3**, 688-694.

Gordon, G. W., Berry, G., Liang, X. H., Levine, B. and Herman, B. (1998). Quantitative fluorescence resonance energy transfer measurements using fluorescence microscopy. *Biophys. J.* **74**, 2702-2713.

Gotz, J., Chen, F., van Dorpe, J. and Nitsch, R. M. (2001). Formation of neurofibrillary tangles in P301l tau transgenic mice induced by Abeta 42 fibrils. *Science* **293**, 1491-1495.

Griesbeck, O., Baird, G. S., Campbell, R. E., Zacharias, D. A. and Tsien, R. Y. (2001). Reducing the environmental sensitivity of yellow fluorescent protein. Mechanism and applications. *J. Biol. Chem.* **276**, 29188-29194.

Hock, C., Konietzko, U., Papassotiropoulos, A., Wollmer, A., Streffer, J., von Rotz, R. C., Davey, G., Moritz, E. and Nitsch, R. M. (2002). Generation of antibodies specific for beta-amyloid by vaccination of patients with Alzheimer disease. *Nat. Med.* **8**, 1270-1275.

Hock, C., Konietzko, U., Streffer, J. R., Tracy, J., Signorell, A., Muller-Tillmanns, B., Lemke, U., Henke, K., Moritz, E., Garcia, E. et al. (2003). Antibodies against beta-amyloid slow cognitive decline in Alzheimer's disease. *Neuron* **38**, 547-554.

Hu, Q., Hearn, M. G., Jin, L. W., Bressler, S. L. and Martin, G. M. (1999). Alternatively spliced isoforms of FE65 serve as neuron-specific and non-neuronal markers. *J. Neurosci. Res.* **58**, 632-640.

Ikeuchi, T. and Sisodia, S. S. (2003). The Notch ligands, Delta1 and Jagged2, are substrates for presenilin-dependent "gamma-secretase" cleavage. *J. Biol. Chem.* **278**, 7751-7754.

Ivics, Z., Hackett, P. B., Plasterk, R. H. and Izsvak, Z. (1997). Molecular reconstruction of Sleeping Beauty, a Tc1-like transposon from fish, and its transposition in human cells. *Cell* **91**, 501-510.

Kim, H. S., Kim, E. M., Lee, J. P., Park, C. H., Kim, S., Seo, J. H., Chang, K. A., Yu, E., Jeong, S. J., Chong, Y. H. et al. (2003). C-terminal fragments of amyloid precursor protein exert neurotoxicity by inducing glycogen synthase kinase-3beta expression. *FASEB J.* **17**, 1951-1953.

Kimberly, W. T., Zheng, J. B., Guenette, S. Y. and Selkoe, D. J. (2001). The intracellular domain of the beta-amyloid precursor protein is stabilized by Fe65 and translocates to the nucleus in a notch-like manner. *J. Biol. Chem.* **276**, 40288-40292.

Kinoshita, A., Whelan, C. M., Smith, C. J., Mikhailenko, I., Rebeck, G. W., Strickland, D. K. and Hyman, B. T. (2001). Demonstration by fluorescence resonance energy transfer of two sites of interaction between the low-density lipoprotein receptor-related protein and the amyloid precursor protein: role of the intracellular adapter protein Fe65. *J. Neurosci.* **21**, 8354-8361.

Kinoshita, A., Whelan, C. M., Smith, C. J., Berezovska, O. and Hyman, B. T. (2002). Direct visualization of the gamma secretase-generated carboxyl-terminal domain of the amyloid precursor protein: association with Fe65 and translocation to the nucleus. *J. Neurochem.* **82**, 839-847.

Kinoshita, A., Shah, T., Tangredi, M. T., Strickland, D. K. and Hyman, B. T. (2003). The intracellular domain of the low density lipoprotein receptor-related protein (LRP) modulates transactivation mediated by APP and Fe65. *J. Biol. Chem.* **278**, 41182-41188.

Lammich, S., Kojro, E., Postina, R., Gilbert, S., Pfeiffer, R., Jasionowski, M., Haass, C. and Fahrenholz, F. (1999). Constitutive and regulated alpha-secretase cleavage of Alzheimer's amyloid precursor protein by a disintegrin metalloprotease. *Proc. Natl. Acad. Sci. USA* **96**, 3922-3927.

Lewis, J., Dickson, D. W., Lin, W. L., Chisholm, L., Corral, A., Jones, G., Yen, S. H., Sahara, N., Skipper, L., Yager, D. et al. (2001). Enhanced neurofibrillary degeneration in transgenic mice expressing mutant tau and APP. *Science* **293**, 1487-1491.

Marambaud, P., Wen, P. H., Dutt, A., Shioi, J., Takashima, A., Siman, R. and Robakis, N. K. (2003). A CBP binding transcriptional repressor produced by the PS1/epsilon-cleavage of N-cadherin is inhibited by PS1 FAD mutations. *Cell* **114**, 635-645.

Matsuda, S., Yasukawa, T., Homma, Y., Ito, Y., Niikura, T., Hiraki, T., Hirai, S., Ohno, S., Kita, Y., Kawasumi, M. et al. (2001). c-Jun N-terminal kinase (JNK)-interacting protein-1b/islet-brain-1 scaffolds Alzheimer's amyloid precursor protein with JNK. *J. Neurosci.* **21**, 6597-6607.

May, P., Reddy, Y. K. and Herz, J. (2002). Proteolytic processing of low density lipoprotein receptor-related protein mediates regulated release of its intracellular domain. *J. Biol. Chem.* **277**, 18736-18743.

Minopoli, G., de Candia, P., Bonetti, A., Faraonio, R., Zambrano, N. and Russo, T. (2001). The beta-amyloid precursor protein functions as a cytosolic anchoring site that prevents Fe65 nuclear translocation. *J. Biol. Chem.* **276**, 6545-6550.

Ni, C. Y., Murphy, M. P., Golde, T. E. and Carpenter, G. (2001). gamma-Secretase cleavage and nuclear localization of ErbB-4 receptor tyrosine kinase. *Science* **294**, 2179-2181.

Ohtsuka, T., Ishibashi, M., Gradwohl, G., Nakanishi, S., Guillemot, F. and Kageyama, R. (1999). Hes1 and Hes5 as notch effectors in mammalian neuronal differentiation. *EMBO J.* **18**, 2196-2207.

Passer, B., Pellegrini, L., Russo, C., Siegel, R. M., Lenardo, M. J., Schettini, G., Bachmann, M., Tabaton, M. and D'Adamio, L. (2000). Generation of an apoptotic intracellular peptide by gamma-secretase cleavage of alzheimer's amyloid beta protein precursor. *J. Alzheimers Dis.* **2**, 289-301.

Ran, Q. and Pereira-Smith, O. M. (2000). Identification of an alternatively spliced form of the Tat interactive protein (Tip60), Tip60(beta). *Gene* **258**, 141-146.

Roncarati, R., Sestan, N., Scheinfeld, M. H., Berechid, B. E., Lopez, P. A., Meucci, O., McGlade, J. C., Rakic, P. and D'Adamio, L. (2002). The gamma-secretase-generated intracellular domain of beta-amyloid precursor protein binds Numb and inhibits Notch signaling. *Proc. Natl. Acad. Sci. USA* **99**, 7102-7107.

Russo, T., Faraonio, R., Minopoli, G., de Candia, P., de Renzis, S. and Zambrano, N. (1998). Fe65 and the protein network centered around the cytosolic domain of the Alzheimer's beta-amyloid precursor protein. *FEBS Lett.* **434**, 1-7.

Sastre, M., Steiner, H., Fuchs, K., Capell, A., Multhaup, G., Condron, M. M., Teplow, D. B. and Haass, C. (2001). Presenilin-dependent gamma-secretase processing of beta-amyloid precursor protein at a site corresponding to the S3 cleavage of Notch. *EMBO Rep.* **2**, 835-841.

Scheinfeld, M. H., Ghersi, E., Laky, K., Fowlkes, B. J. and D'Adamio, L. (2002a). Processing of beta-amyloid precursor-like protein-1 and -2 by gamma-secretase regulates transcription. *J. Biol. Chem.* **277**, 44195-44201.

Scheinfeld, M. H., Roncarati, R., Vito, P., Lopez, P. A., Abdallah, M. and D'Adamio, L. (2002b). Jun NH2-terminal kinase (JNK) interacting protein 1 (JIP1) binds the cytoplasmic domain of the Alzheimer's beta-amyloid precursor protein (APP). *J. Biol. Chem.* **277**, 3767-3775.

Scheinfeld, M. H., Matsuda, S. and D'Adamio, L. (2003). JNK-interacting protein-1 promotes transcription of A beta protein precursor but not A beta precursor-like proteins, mechanistically different than Fe65. *Proc. Natl. Acad. Sci. USA* **100**, 1729-1734.

Schroeter, E. H., Kisslinger, J. A. and Kopan, R. (1998). Notch-1 signalling requires ligand-induced proteolytic release of intracellular domain. *Nature* **393**, 382-386.

Selkoe, D. J. (1999). Translating cell biology into therapeutic advances in Alzheimer's disease. *Nature* **399**, 23-31.

Shearman, M. S., Beher, D., Clarke, E. E., Lewis, H. D., Harrison, T., Hunt, P., Nadin, A., Smith, A. L., Stevenson, G. and Castro, J. L. (2000). L-685,458, an aspartyl protease transition state mimic, is a potent inhibitor of amyloid beta-protein precursor gamma-secretase activity. *Biochemistry* **39**, 8698-8704.

Shivers, B. D., Hilbich, C., Multhaup, G., Salbaum, M., Beyreuther, K. and Seeburg, P. H. (1988). Alzheimer's disease amyloidogenic glycoprotein: expression pattern in rat brain suggests a role in cell contact. *EMBO J.* **7**, 1365-1370.

Sisodia, S. S. and St George-Hyslop, P. H. (2002). gamma-Secretase, Notch, Abeta and Alzheimer's disease: where do the presenilins fit in? *Nat. Rev. Neurosci.* **3**, 281-290.

Sterner, D. E. and Berger, S. L. (2000). Acetylation of histones and transcription-related factors. *Microbiol. Mol. Biol. Rev.* **64**, 435-459.

Suhr, S. T., Gil, E. B., Senut, M. C. and Gage, F. H. (1998). High level transactivation by a modified Bombyx ecdysone receptor in mammalian cells without exogenous retinoid X receptor. *Proc. Natl. Acad. Sci. USA* **95**, 7999-8004.

Taru, H. and Suzuki, T. (2004). Facilitation of stress-induced phosphorylation of beta-amyloid precursor protein family members by X11-like/MINT2 protein. *J. Biol. Chem.* **279**, 21628-21636.

Taru, H., Iijima, K., Hase, M., Kirino, Y., Yagi, Y. and Suzuki, T. (2002a). Interaction of Alzheimer's beta-amyloid precursor family proteins with scaffold proteins of the JNK signaling cascade. *J. Biol. Chem.* **277**, 20070-20078.

Taru, H., Kirino, Y. and Suzuki, T. (2002b). Differential roles of JIP scaffold proteins in the modulation of amyloid precursor protein metabolism. *J. Biol. Chem.* **277**, 27567-27574.

Vassar, R., Bennett, B. D., Babu-Khan, S., Kahn, S., Mendiaz, E. A., Denis, P., Teplow, D. B., Ross, S., Amarante, P., Loeloff, R. et al. (1999). Beta-secretase cleavage of Alzheimer's amyloid precursor protein by the transmembrane aspartic protease BACE. *Science* **286**, 735-741.

Walsh, D. M., Fadeeva, J. V., LaVoie, M. J., Paliga, K., Eggert, S., Kimberly, W. T., Wasco, W. and Selkoe, D. J. (2003). gamma-Secretase cleavage and binding to FE65 regulate the nuclear translocation of the intracellular C-terminal domain (ICD) of the APP family of proteins. *Biochemistry* **42**, 6664-6673.

Walter, J., Kaether, C., Steiner, H. and Haass, C. (2001). The cell biology of Alzheimer's disease: uncovering the secrets of secretases. *Curr. Opin. Neurobiol.* **11**, 585-590.

Whitmarsh, A., Cavanagh, J., Tournier, C., Yasuda, J. and Davis, R. (1998). A mammalian scaffold complex that selectively mediates MAP kinase activation. *Science* **281**, 1671-1674.

Xia, Z. and Liu, Y. (2001). Reliable and global measurement of fluorescence resonance energy transfer using fluorescence microscopes. *Biophys. J.* **81**, 2395-2402.

Xiao, H., Chung, J., Kao, H. Y. and Yang, Y. C. (2003). Tip60 is a co-repressor for STAT3. *J. Biol. Chem.* **278**, 11197-11204.